

Parametric versus non-parametric modelling? Statistical evidence based on P -value curves.

Nicolai Bissantz¹, Axel Munk¹ and Achim Scholz^{1,2}

¹*Institut für Mathematische Stochastik, Universität Göttingen, Lotzestr.13, D-37083 Göttingen, Germany*

²*Citibank Privatkunden AG, Düsseldorf, Germany*

6 November 2018

ABSTRACT

In astrophysical (inverse) regression problems it is an important task to decide whether a given parametric model describes the observational data sufficiently well or whether a non-parametric modelling becomes necessary. However, in contrast to common practice this cannot be decided by solely comparing the quality of fit due to possible over-fitting by the non-parametric method. Therefore, in this paper we present a re-sampling algorithm which allows to decide whether deviations between a parametric and a non-parametric model are systematic or due to noise. The algorithm is based on a statistical comparison of the corresponding residuals, under the assumption of the parametric model as well as under violation of this assumption. This yields a graphical tool for a robust decision making of parametric versus non-parametric modelling.

Moreover, our approach can be used for the selection of the most proper model among several competitors (model selection). The methods are illustrated by the problem of recovering the luminosity density in the Milky Way [MW] from near-infrared [NIR] surface brightness data of the *DIRBE* experiment on board of the *COBE* satellite. Among the parametric models investigated one with 4-armed spiral structure performs best. In this model the Sagittarius-Carina arm and its counter-arm are significantly weaker than the other pair of arms. Furthermore, we find statistical evidence for an improvement over a range of parametric models with different spiral structure morphologies by a non-parametric model of Bissantz & Gerhard (2002).

Key words: methods: data analysis - methods: statistical - Galaxy: disc - Galaxy: structure.

1 INTRODUCTION

One of the basic problems in astrophysical research consists in the proper choice of a model to describe an observational array $\omega_{\text{obs}}(t_i), i = 1, \dots, N$ of N measurements. Here $t = (t_1, \dots, t_N)$ denotes a quantity which affects $\omega = (\omega(t_1), \dots, \omega(t_N))$ in a systematic, but blurred way, $\omega(t_i)$, the regression function to be reconstructed from the data. For example, $\omega_{\text{obs}}(t_i)$ could be measurements of the surface brightness at sky position $t_i = (l_i, b_i)$. In noisy inverse models ω itself is not the quantity of primary interest, rather a function ρ has to be recovered, where the relation between ω and ρ is given by a (linear) operator K (matrix), viz.

$$\omega(t_i) = (K\rho)(t_i), \quad i = 1, \dots, N.$$

Often K is given by a $N \times N$ matrix, which will in general be numerically difficult to invert. This will also be the case in this paper where we are concerned with the recovery of the spatial (three-dimensional) luminosity density of a galaxy from blurred observations of its surface brightness and reverberation mapping of gas in AGNs. For more examples of inverse problems in astrophysics see e.g. Lucy (1994). Due to the noisy measurements it is tempting to assume that $\omega_{\text{obs}}(t_i) = \omega(t_i) + \varepsilon_i$, where the ε_i denote some random noise and $\omega(t_i)$ the expected value of $\omega_{\text{obs}}(t_i)$, i.e. $E[\omega_{\text{obs}}(t_i)] = \omega(t_i)$. In particular we allow for different error distributions of the ε_i , which entails inhomogeneous variance patterns (cf. Hocking, 1996, for a thorough discussion of models with inhomogeneous variances), viz. $V[\varepsilon_i] = \sigma_i^2$, as will be the case in our example of de-projecting the de-reddened *COBE/DIRBE* L-band surface brightness map of

Spiegel et al. (1995). Cf. Bissantz & Munk, (2001) [BM1] for the noise properties of this data.

In this paper we are concerned with a new method to compare several competing models for the regression function ρ and to select the most appropriate one. These models may be of a certain parametric form (parametric model)

$$U = \{\rho_\vartheta\}_{\vartheta \in \Theta}, \quad \Theta \subseteq \mathbb{R}^d$$

or non-parametric, i.e. only qualitative smoothness or geometric assumptions such as symmetry or differentiability, (cf. Wand & Jones (1995) or Wahba (1990) for a good introduction to non-parametric modelling by kernel or spline methods, respectively) are made a-priori. Implicitly, any algorithm, to reconstruct ρ from ω , relies on those assumptions or combinations thereof. Statistical methods for model selection are broadly used in astrophysics (cf. Feigelson & Babu, 2002), a good statistical introduction into this area is Burnham & Anderson (1998) or Eubank (1999) among many others. The case of inhomogeneous inverse models, as in our application, is not treated explicitly in the literature so far.

Our approach is based on the statistical comparison of the estimated parametric residuals

$$\hat{\varepsilon}_i = \omega_{\text{obs}}(t_i) - (K\rho_{\hat{\rho}})(t_i), \quad i = 1, \dots, N,$$

where $\rho_{\hat{\rho}}$ denotes the best possible fit of the model class U to the data ω_{obs} (e.g. obtained by least squares), and the estimated non-parametric residuals

$$\varepsilon_i^{(\text{np})} = \omega_{\text{obs}}(t_i) - (K\rho^{(\text{np})})(t_i), \quad i = 1, \dots, N,$$

where $\rho^{(\text{np})}$ denotes a non-parametric reconstruction of ρ . This estimator can be obtained by several methods, including penalized maximum likelihood if the error distribution of ε is known (e.g. Magorrian et al., (1998), Bissantz & Gerhard, 2002), the Richardson-Lucy iterative method (e.g. Binney, Gerhard & Spiegel, 1997 [BGS]), subtractive optimally localized averages (e.g. Pijpers & Thompson, 1994, Pijpers & Wanders, 1994), and maximum entropy methods (e.g. Wallington et al., 1994, 1996).

In our example, which will be discussed in detail in Sect. 4 and 5, a penalized maximum likelihood method is used, where the penalty terms encourage symmetry, smoothness features and spiral structure of the recovered density distribution. In this model the error distribution is assumed to be independent of the data point.

Now the general methodology will be to use the difference of the residuals $\hat{\varepsilon}_i$ and $\varepsilon_i^{(\text{np})}$

$$\hat{\delta}_i = \hat{\varepsilon}_i - \varepsilon_i^{(\text{np})} = (K\rho_{\hat{\rho}} - K\rho^{(\text{np})})(t_i).$$

Roughly speaking, a small sum of squares of $\hat{\delta}_i$ will indicate that the non-parametric and the parametric fit are close, which should give evidence for the parametric model to hold. Otherwise, if $\frac{1}{N} \sum \hat{\delta}_i^2$ is large the non-parametric fit outperforms the parametric one. Due to the possibly inhomogeneous variance pattern of the error σ_i^2 , a valid statistical

analysis requires that $\hat{\delta}_i$ has to be weighted with the estimated local variability $\hat{\sigma}_i^2 = \sigma^2(t_i)$, which results in a locally weighted residual sum of squares

$$\text{LWRSS} = \frac{1}{N} \sum_{i=1}^N \left(\frac{\hat{\varepsilon}_i - \varepsilon_i^{(\text{np})}}{\hat{\sigma}_i} \right)^2.$$

Observe, that the use of the locally weighted residual sums of squares leads to a quantity which does not depend on the (unknown) local variability of the data, i.e.

$E \left[(\hat{\varepsilon}_i - \varepsilon_i^{(\text{np})}) / \hat{\sigma}_i \right]^2$ will be a quantity which is independent of σ_i^2 for large N . In fact, we claim that under certain regularity conditions on K , the error distribution of ε , σ and ρ , $N\sqrt{h_N}\text{LWRSS}$ has a normal limit, where h_N is a sequence tending to zero as $N \rightarrow \infty$. Hence the distribution of $N\sqrt{h_N}\text{LWRSS}$ for large numbers of observations tends to be asymptotically normal with a rather complicated variance which will depend on K , σ and the smoothing method used for obtaining $\hat{\rho}$. For the case of direct regression (then K is the identity) this was made explicit by Dette (1999) and Dette & Munk (2002), where we claim that the proof in the indirect case follows a similar pattern, and is postponed to a different paper. In order to base a proper decision whether $\rho_{\hat{\rho}}$ is acceptable or $\rho^{(\text{np})}$ should be preferred, the approximate normal distribution of $N\sqrt{h_N}\text{LWRSS}$ can now be used. The only problem which remains is to determine the variance of $N\sqrt{h_N}\text{LWRSS}$ which will be done in the sequel by a resampling (bootstrap) algorithm from the data. Various simulation studies have shown that this method even leads to a better approximation of the true distribution of RSS (for finite N) than the asymptotic ($N \rightarrow \infty$) normal law. This is in accordance with work of Dette, von Lieres und Wilkau & Sperlich (2001), who investigated various variants of this algorithm in a different context and came to the same conclusion. Our bootstrap algorithm will be presented in Sect. 3.

In Sect. 5 we apply the algorithm to the analysis of a dust-corrected near-infrared [NIR] *COBE/DIRBE* L-band map of the Milky Way [MW] (Spiegel et al., 1995). Bissantz & Gerhard (2002) modelled this data non-parametrically with an implementation of the penalized maximum likelihood method. We find that their model improves significantly on various parametric models constructed from the parametric model of the same data [BGS], supplemented by different spiral structure models (cf. Sect. 4 for a description). By our method it can be concluded that this improvement in fit is not due to overfitting of the data, but rather to systematic departures between data and parametric models, which are in particular not flexible enough to capture certain deviations from a double-exponential disk and smooth spiral arms.

We mention that our method can be used as well to decide between several classes of concurring parametric models (with possibly different numbers of parameters). Among the parametric models with different spiral structure that we have investigated, a four-armed model with the Sagittarius-

Carina arm (and its counter-arm) significantly weaker than the other arms (cf. Drimmel & Spergel, 2001), outperforms its competitors.

Finally, we mention that the main difference of our method to previous work of the authors ([BM1], Bissantz & Munk, 2002 [BM2]) consists in three important aspects. First, LWRSS adapts to local variability estimated from data, which yields an overall measure of goodness of fit weighting the impact of data due to its local variability. Our numerical analysis shows that this yields much more reliable results as before. Second, we do not require an additional smoothing step for the residual differences as in [BM2]. This smoothing step had to be introduced in [BM1] in order to obtain a distributional limit of the statistic considered there. However, due to this additional smoothing the statistics becomes much harder to interpret. In the present approach this is not necessary anymore, and our statistics LWRSS measures asymptotically the L^2 -distance between the true model ρ and the parametric model ρ_θ , i.e.

$$M^2 = \min_{\theta \in \Theta} \|K(\rho - \rho_\theta)\|^2$$

where $\|\cdot\|$ refers to the euclidian norm. Furthermore, our new method also allows comparison with a non-parametric competitor, which serves as an objective alternative.

For those readers, who are mainly interested in the methodological part of this paper we recommend to skip Sect. 4.

2 A NEW STATISTICAL METHOD TO DECIDE BETWEEN PARAMETRIC AND NON-PARAMETRIC MODELLING

As mentioned in the introduction the underlying idea of our approach is to base the decision, whether the model U should be considered as acceptable, on the LWRSS, which has to be computed in the following steps. We illustrate our algorithm for the case where t_i are located on a two-dimensional grid as it will be the case in our example in Sect. 4.

(i) (Computation of the residual difference). Observe, that $\hat{\varepsilon}_i - \varepsilon_i^{(\text{np})} = \omega_{\hat{j}} - \omega^{(\text{np})}$.

(ii) (Computation of a local estimate $\hat{\sigma}^2$ of the variance σ^2). Here, several methods are appropriate. A simple method is based on Savitzky-Golay filters (Press et al., 1994), which are common in astrophysics. The method requires the computation of the differences between a non-parametric model and the observed data at 7 neighbouring points on a grid:

$$\hat{\sigma}^2(l_i, b_j) = \sum_{k=-2}^2 c_k \left\{ \sum_{l=-2}^2 c_l \left(\omega^{(\text{np})}(l_{i+l}, b_{j+k}) - \omega_{\text{obs}}(l_{i+l}, b_{j+k}) \right)^2 \right\}$$

$$i = 3, \dots, n-2 \quad \text{and} \quad j = 3, \dots, m-2$$

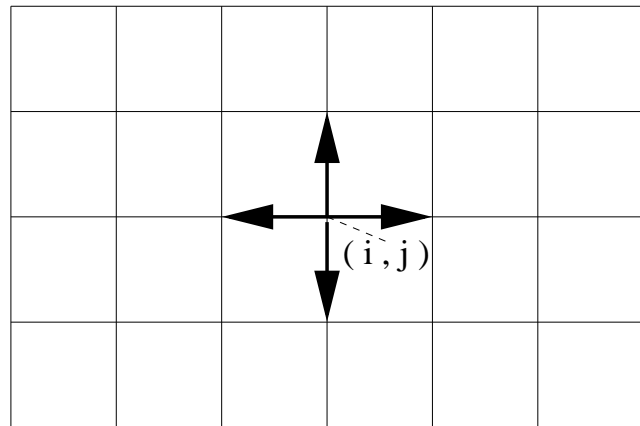


Figure 1. Local residuals required for estimating the variance σ^2 .

where the $\omega_{\text{obs}}(l_i, b_j)$, $\begin{matrix} i=1, \dots, n \\ j=1, \dots, m \end{matrix}$ are the observations, the c_k and c_l are weights chosen according to a Savitzky-Golay filter (Press et al., 1994, setting $n_L = n_R = M = 2$) and $\omega^{(\text{np})}$ is a non-parametric model of the Milky Way.

Further approaches in the estimation of the local variability are possible with methods based on the computation of the local differences of, say 4, neighbouring points on a grid (cf. Fig. 1):

$$\hat{\sigma}_{ij}^2 = \frac{1}{8} \left\{ \sum_{k=-1}^1 (\omega_{\text{obs}}(l_i, b_j) - \omega_{\text{obs}}(l_{i+k}, b_j))^2 + \sum_{k=-1}^1 (\omega_{\text{obs}}(l_i, b_j) - \omega_{\text{obs}}(l_i, b_{j+k}))^2 \right\},$$

$$i = 2, \dots, n-1 \quad \text{and} \quad j = 2, \dots, m-1.$$

Then, in a second step the average over a window of neighbouring local residuals $\hat{\sigma}_{ij}^2$ is computed, viz.

$$\hat{\sigma}^2 \equiv \sum_{i,j=-r,-s}^{r,s} \hat{\sigma}_{ij}^2,$$

where the window size can be chosen according to prior information on constant regions of the expected local variability.

Better but more computer intensive methods can be obtained by applying a kernel estimator to the residual squares $\hat{\varepsilon}_i^2$, see e.g. Ruppert et al. (1997), or biased reduced variance estimators (Thompson et al., 1991, Munk et al., 2001).

(iii) (Compute LWRSS). Now, the distribution of LWRSS is required, which is extremely difficult to compute explicitly. See, e.g. for the case of a direct regression model, Dette (1999). Nevertheless, in the following we describe a resampling algorithm which performs well. Numerical investigations have shown (cf. Dette, 1999, and Dette et al., 2001) that a modification of the wild bootstrap approximates the true distribution of LWRSS very well and a bootstrap limit law has been proved in Dette & Neumeyer (2001) in a similar but simpler context. Even for rather small numbers of observations, $N = 100$, say, these authors found in a broad

range of scenarios on the error distribution and ρ satisfactory results. This is in accordance with our findings.

3 PERFORMING THE BOOTSTRAP ALGORITHM

Our proposed algorithm is a modification of the algorithm presented in Bissantz & Munk (2001), and consists of the following steps.

Step 0: Compute $\omega^{(\text{np})}$.

Step 1: (*Generate random data*). Generate N random data $\omega_{\text{obs}}^{(i)}$ by drawing with replacement from the observed data ω_{obs} .

Step 2: (*Fitting of the random data*). Determine the "parametrically best-fitting model" $\rho_{\hat{\theta}^{(i)}}$ of the random data $\omega_{\text{obs}}^{(i)}$.

Step 3: (*Compute the target*). Compute the LWRSS $\hat{M}_{(i)}^2 = \|\omega_{\hat{\theta}^{(i)}} - \omega^{(\text{np})}\|_{\text{LWRSS}}^2$ (see below for the formal definition of this distance measure).

Step 4: (*The replication process*). Repeat steps 1 – 3 B times. This yields values $\hat{M}_{(1)}^2, \dots, \hat{M}_{(B)}^2$. B is a large number, with $B \approx 500 - 1000$ usually sufficient. In contrast to [BM2] the non-parametric fit $\omega^{(\text{np})}$ is kept fixed, whereas the parametric fit is randomly perturbed in this algorithm. This leads to a significant reduction of computing time.

Observe that $\hat{M}_{(1)}^2, \dots, \hat{M}_{(B)}^2$ are realisations of a random quantity $X = \hat{M}_*^2$, and the cumulative distribution function F_B^* approximates the distribution function F of \hat{M}^2 .

This algorithm is in accordance with the algorithm of Dette et al. (2001) who suggested this method in a different context. Interestingly, these authors came to the same conclusion, that bootstrapping from the parametric model gives much more reliable results than bootstrapping from the non-parametric residuals $\varepsilon_i^{(\text{np})}$. This is an empirical finding and somehow in contrast to theoretical results.

4 NEAR-INFRARED MODELS OF THE MILKY WAY

We now apply our proposed method to models of *COBE/DIRBE* NIR data in the following. Such models of the distribution of near-infrared luminosity in the inner MW are particularly interesting because NIR light traces luminous mass well (e.g. Rix & Zaritzky, 1995). *COBE/DIRBE* NIR maps were used to estimate the NIR luminosity distribution both parametrically (e.g. Freudenreich, 1998, Dwek et al., 1995, and Drimmel & Spergel, 2001), and non-parametrically ([BGS], Bissantz, Englmaier, Binney & Gerhard, 1997, and Bissantz & Gerhard, 2002). Only the models of Drimmel & Spergel (2001) and Bissantz & Gerhard (2002) contain spiral arms. Bissantz & Gerhard (2002) show that inclusion of spiral structure is important for the bar/bulge

of the model, as only then the elongation of the bulge/bar in their models is large enough to reproduce clump giant star count data of Stanek et al. (1994, 1997). Such star count data contain information about the distances to the surveyed stars, complementary to the all-sky coverage of the *COBE/DIRBE* NIR map; thus the star count data provides an important *a posteriori* test of the model(s).

However, despite of its importance, the morphology of the stellar spiral arms of the Milky Way (i.e. in the distribution of luminous mass) is not well known. In particular it is unclear whether it is predominantly 2- or 4-armed. Ortiz & Lépine (1993) used a 4-armed model with logarithmic spiral structure in their model of MW NIR starcounts. However, there is a tangent point at ≈ 49 deg in the (very probably 4-armed) distribution of gas and dust (Englmaier & Gerhard, 1999), which seems to be missing in the *COBE/DIRBE* K-band map of the MW (Drimmel, 2000). This indicates 2-armed rather than 4-armed structure. On the other hand this tangent is also weak in CO, possibly due to the geometry of the line-of-sight through this arm (Dame, private communication). In Drimmel & Spergel (2001) the analysis of the *COBE/DIRBE* 240 μm (tracing dust) and NIR (tracing stellar light) data was extended, and a combined dust and stellar disk model produced. The authors found a best model for the stellar disk which is 4-armed. However, the Sagittarius-Carina arm in their model is weaker by a factor of 0.4 in arm-interarm density contrast than the other arms. Bissantz & Gerhard (2002) found in their non-parametric reference model with spiral arms that inclusion of spiral structure significantly improves their model, however they were not able to decide whether 2 or 4-armed structure is preferable.

Here we aim to better understand stellar spiral structure in the MW by further analysis of a dust-corrected *COBE/DIRBE* L-band map (Spergel et al. 1995), shown in Fig. 2. For our analysis we compare four classes of parametric models based on this data, which differ with regard to the spiral structure. We include models with 2-arms, with 4-arms, without arms and an intermediate model consisting of a strong and a weak pair of arms (the latter model as suggested by Drimmel & Spergel, 2001).

We apply our proposed statistical method to perform the comparison of the parametric models by using the non-parametric reference model of Bissantz & Gerhard (2002) as an objective standard of measurement. To this end the P -value curves of [BM2] are modified for the LWRSS-statistic. Additionally, with our methodology we find that the non-parametric model better reproduces the informative part of the L-band map than the best parametric model, particularly in the disk near spiral arm tangent point features (cf. Fig. 5). This is achieved by using the distribution of LWRSS which is found by the bootstrap algorithm in Sect. 3. In fact this shows that there is rare evidence that the difference between the parametric and non-parametric fit is solely due to noise, rather than due to a systematic departure of the

COBE/DIRBE L-band data

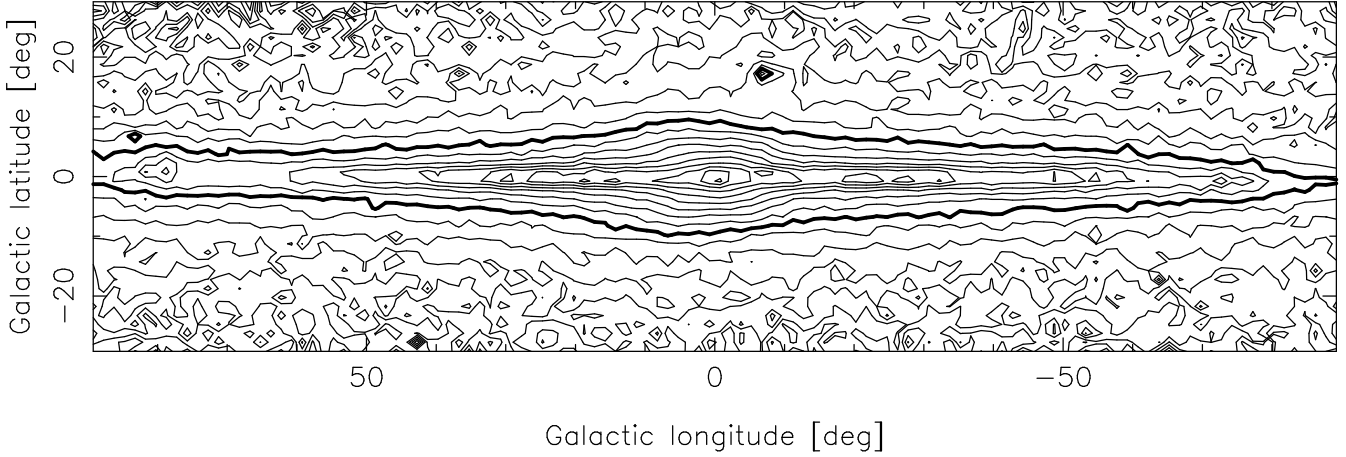


Figure 2. The dust-corrected *COBE/DIRBE* L-band map of Spergel et al. (1995). Contour spacing is 0.5mag^2 and the bold contour is at 0mag^2 . Note that there is an arbitrary offset to this scale, however it is the same as used in Fig. 5 to allow for a comparison of models and data.

true ρ and the best parametric model as described in the last paragraph.

First we introduce the parametric models in Sect. 4.1 and the non-parametric reference model of Bissantz & Gerhard (2002) in Sect. 4.2.

4.1 The parametric models

The parametric models are defined on a Galacto-centric Cartesian coordinate system with axes x, y, z , where x is along the major axis, and y along the minor axis of the bulge/bar, both in the main plane of the MW. The position of the Sun in this coordinate system is $z_{\odot} = 14\text{pc}$ above the main plane of the disk and $R_{\odot} = 8\text{kpc}$ from the Galactic centre, and the angle between the major axis of the bar and the line-of-sight from the Sun to the Galactic Centre is $\phi_{\text{bar}} = 20\text{deg}$ [BGS].

The parametric models analysed in this paper are similar, except for their spiral structure. The other model constituents are a double-exponential disk and a truncated power-law bulge (cf. [BGS]). Calling the disk density ρ_d and the bulge density ρ_b we define the model density ρ as:

$$\rho(\vec{x}) = \rho_d(\vec{x}) + \rho_b(\vec{x}), \quad (1)$$

where

$$\rho_d \equiv \rho_d^0 \cdot R_d \cdot e^{-R/R_d} \cdot \left(\frac{e^{-|z|/z_0}}{z_0} + \alpha \frac{e^{-|z|/z_1}}{z_1} \right),$$

$$\rho_b \equiv \frac{\rho_b^0}{\eta \zeta a_m^3} \cdot \frac{e^{-a^2/a_m^2}}{(1 + a/a_0)^{1.8}},$$

$$a \equiv \sqrt{x^2 + \frac{y^2}{\eta^2} + \frac{z^2}{\zeta^2}}, \quad R \equiv \sqrt{x^2 + y^2} \quad \text{and} \quad \vec{x} = (x, y, z).$$

Bissantz & Gerhard (2002) added 4-armed spiral structure to this density ρ , according to the model of Ortiz & Lépine (1993), and then used the model as initial model in their non-parametric de-projection. The positions of the spiral arms $r_i(\phi)$ ($i = 1, \dots, 4$) in the model of Ortiz & Lépine (1993) are given by

$$r_i(\phi) = 2.33\text{kpc} \cdot e^{(\phi - \phi_{\text{bar}} - \phi_i) \cdot \tan(\chi)},$$

where the angle $\phi_i = 0, \pi/2, \pi, 3\pi/2$ determines the innermost position angle of a spiral arm in Galacto-centric coordinates with respect to the major axis of the bar, and $\chi = 13.8\text{deg}$ is the pitch angle of the arms.

In our parametric models the spirals exist between Galactocentric radius of 3.5 kpc, which is the approximate outer extend of the bar/bulge (Bissantz & Gerhard, 2002), and an outer radius of 10 kpc. The spiral arms are modelled by a Gaussian profile with full width at half maximum $\approx 300\text{pc}$ (Ortiz & Lépine, 1993). We treat the spiral arms as enhancements of the disc density. The only free parameter that we fit for the spiral structure is the amplitude d_s of the density modulations:

$$\rho_d^{\text{including spiral}} = \rho_d \cdot \prod_{i=1}^4 \left(1 + d_s \cdot e^{-\ln(2) \cdot \Delta r_i^2 / (0.5 \cdot \text{FWHM})^2} \right),$$

where Δr_i is the (approximate) distance to the nearest point along spiral arm i . To keep the problem computationally tractable we use this rather simple model of the spiral structure in the following. Note that Vallée (2002) suggests some improvements to the model of Ortiz & Lépine, however there is good agreement between these models in the radial range $3\text{kpc} \leq r \leq 6\text{kpc}$ from the Galactic Center. This is where most of the evidence results for spiral structure in the subsequently analysed region of the sky (cf. Sect. 5.1). Also visual inspection of the residuals of all parametric models showed

no systematic deviations between the position of model spiral arm tangent points from those in the data.

We call this 4-armed model "model A" in the subsequent analysis. The other parametric models under investigation are modifications of model "A". Model "B" has no spiral arms at all, and in model "C" we omit the Sag-Car-arm and its counter-arm, as suggested by Drimmel (2000). Finally, in our "intermediate" model "D" the amplitude d_s of the Sag-Car arm and its counter-arm are a factor of 0.4 smaller than the amplitude of the other pair of arms, as suggested by Drimmel & Spergel (2001).

4.2 The non-parametric model

As a non-parametric competitor to the above mentioned parametric models we use the reference non-parametric luminosity density model of Bissantz & Gerhard (2002). It was estimated from the dust-corrected *COBE/DIRBE* L-band map of Spergel et al. (1995), using a penalised maximum likelihood algorithm with penalty terms that encourage in the model density eightfold-symmetry with respect to the three main planes of (approximate) symmetry of the bar, smoothness, and spiral structure (similar to the 4-armed spiral structure of the Ortiz & Lépine, 1993, model). The non-parametric model is defined on a (Galactocentric) grid of $60 \times 60 \times 41$ grid points which extends 10 kpc along the x and y axis, and 3 kpc along the z -axis. Outside of this box the model is continued by a parametric model of the L-band map.

Bissantz & Gerhard (2002) derived non-parametric models for bar angles $10 \text{ deg} \leq \varphi_{\text{bar}} \leq 44 \text{ deg}$. They found a preferred range of bar angles $20 \text{ deg} \leq \varphi_{\text{bar}} \leq 25 \text{ deg}$. Their best model is for bar angle $\varphi_{\text{bar}} = 20 \text{ deg}$, and is the "reference" model analysed subsequently.

5 APPLICATION TO MODELS OF THE MILKY WAY

In this section we describe the application of our statistical method to MW models A-D. To this end we estimate M^2 , which is the distance between the "true" MW density ρ , and the "best-fitting" parametric model $\rho_{\hat{\theta}^*}$, of each of the model (classes) A-D. Note that we use the reference non-parametric model as an objective standard of measurement. We approximately determine the statistic of M^2 by bootstrap replication of the distance $\hat{M}_{(i)}^2$ (in our case $i = 1, \dots, \approx 1000$) between "best fitting" models $\rho_{\hat{\theta}^{(i)}}$ of random data $\omega_{\text{obs}}^{(i)}$ and the non-parametric reference model $\omega^{(np)}$ (cf. Sect. 3). The random data $\omega_{\text{obs}}^{(i)}$ is generated from the *COBE/DIRBE* data ω_{obs} by drawing with replacement. We describe in this section the generation of the random sets of data (Sect. 5.1), the computation of $\hat{M}_{(i)}^2$ (Sect. 5.2), and finally, in Sect. 5.3, we explain how to evaluate the resulting statistic of $\hat{M}_{(i)}^2$ for the parametric models.

5.1 Random data sets based on the *COBE/DIRBE* data

We construct random sets of data $\omega_{\text{obs}}^{(i)}$ from a subset of the Spergel et al. (1995) *COBE/DIRBE* data which is generated in a first step as follows: We linearly interpolate the surface brightness data (in magnitudes) on a grid \mathcal{G} with $N = 4800$ equidistant points, covering $|l| \leq 40 \text{ deg}$, $|b| \leq 10 \text{ deg}$ from the observed data. We restrict the data to this area because there the parametric continuation of the non-parametric model contributes only unimportantly to the projection of the model to the sky.

In the second step we estimate the local noise properties of the *COBE/DIRBE* data on the grid \mathcal{G} . To this end we compute a map of the square difference between the projection of the non-parametric reference model to the sky and the *COBE/DIRBE* data (both in magnitudes) at those positions of the sky where this data is available. Then we smooth this map, employing a Savitzky-Golay filter (Press et al., 1994, setting $n_R = n_L = M = 2$ for their parameters). This procedure yields a non-parametric estimate of the local variance $\hat{\sigma}^2(l, b)$ (cf. Sect. 2). Finally, we determine the local variance at the points of grid \mathcal{G} by linear interpolation in this map.

In our final step we construct random data $\omega_{\text{obs}}^{(i)}$ as follows. We randomly draw *with replacement* 4800 points (l_j, b_j) out of the grid \mathcal{G} . The surface brightness observations $\omega_{\text{obs}}(l_j, b_j)$ together with the estimates of the local variance $\hat{\sigma}^2(l_j, b_j)$, at the drawn points (l_j, b_j) , then constitute a random sample of data. Observe, that drawing with replacement implies that a point (l_j, b_j) may occur more than once in this random sample.

5.2 The distribution of $\hat{M}_{(i)}^2$

We approximate the statistic of the distance between the best-fitting parametric model $\rho_{\hat{\theta}}$ for every parametric model A-D and the reference non-parametric model as follows. We compute $B = 1000$ bootstrap replications of $\hat{M}_{(i)}^2$, using the following procedure for $1 \leq i \leq 1000$:

(i) Generation of a random set of data $\omega_{\text{obs}}^{(i)}$ from the *COBE/DIRBE* L-band data (cf. Sect. 5.1).

(ii) Determination of the weighted least square estimator (WLSE) $\hat{\theta}^{(i)}$ (the best-fitting model) for this random data set. For this we use a Marquardt-Levenberg-algorithm (Press et al., (1994)), which was used to minimize the distance

$$\sum_{\text{all points } (l, b)_j \text{ of } \omega_{\text{obs}}^{(i)}} \frac{\left(\omega_{\text{obs}}^{(i)}((l, b)_j) - \omega_{\hat{\theta}}((l, b)_j) \right)^2}{\hat{\sigma}^2((l, b)_j)}.$$

For the computation of $\hat{\sigma}^2$ see (ii) in Sect. 2. The fitting is done in a two-step process:

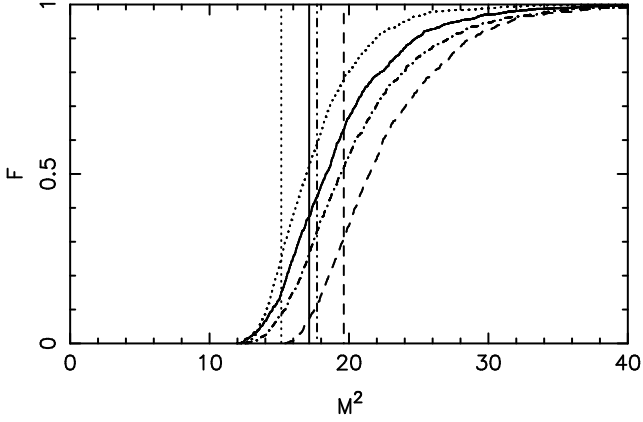


Figure 3. Cumulative distribution functions of $\hat{M}_{(i)}^2$ for models A (full line), B (dashed), C (dot-dash-dot-dash) and D (dotted). The vertical line indicates the distance \hat{M}^2 of the best-fitting parametric model $\rho_{\hat{\theta}}$ for the original *COBE/DIRBE* data from the non-parametric model.

1. Fitting of the disk parameters: In the first step we fit the disk parameters and the bulge normalisation b , with the other bulge parameters fixed.

2. Fitting of the bulge/bar parameters: In the second step we fix the disk related parameters found in the first step (except for the normalisation parameter d) and fit the bulge/bar parameters and d .

(iii) Computation of the distance $\hat{M}_{(i)}^2$ between the reference non-parametric model and the best-fitting parametric model $\hat{\theta}^{(i)}$:

$$\begin{aligned} \hat{M}_{(i)}^2 &= \|\omega_{\hat{\theta}^{(i)}} - \omega^{(\text{np})}\|^2 \\ &= \frac{1}{n \cdot m} \sum_{\substack{\text{all points} \\ ((l, b)_j) \text{ of } \mathcal{G}}} \left(\frac{\omega_{\hat{\theta}^{(i)}}((l, b)_j) - \omega^{(\text{np})}((l, b)_j)}{\hat{\sigma}^2((l, b)_j)} \right)^2, \end{aligned}$$

where $n \cdot m = 4800$.

From the $B = 1000$ bootstrap replications $\hat{M}_{(i)}^2$ we then determine the empirical cumulative probability distribution function of the random quantity \hat{M}_*^2 , shown in Fig. 3, for the parametric models A-D. Also indicated in Fig. 3 are the estimated distances \hat{M}^2 between the non-parametric model and the best-fitting parametric models $\rho_{\hat{\theta}}$ of the *COBE/DIRBE* surface brightness, restricted to the grid \mathcal{G} , which is computed from the observed *COBE/DIRBE* data.

5.3 P -value curves: Interpretation of the numerical results

We now proceed by using the bootstrap replications for the parametric models A-D to answer two fundamental questions:

(i) Should the non-parametric model be preferred over the parametric models, i.e. does it improve the fit to the informative part (signal) of the data?

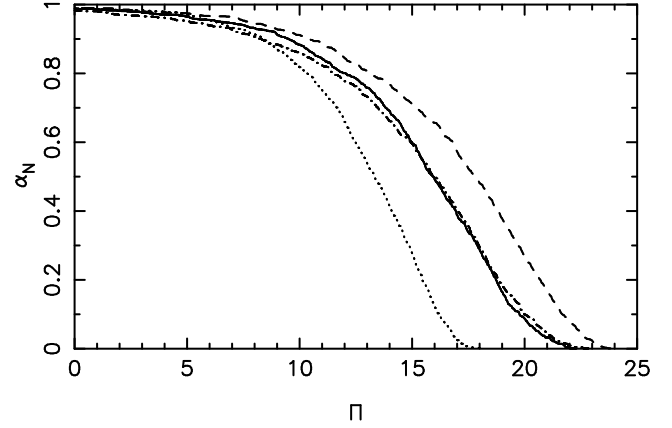


Figure 4. P -value curves $\alpha_N(\Pi) = F_B^*(\hat{M}^2 - \Pi)$ for models A (full line), B (dashed), C (dot-dash-dot-dash), and D (dotted).

(ii) How do the parametric models compare to each other, can we decide for a "best" among them, and - if yes - which one is it?

We begin with some general remarks on our proposed method before we use it to answer these questions. The main methodology we propose is the use of P -value curves for the distance M^2 as graphical tools for illustrating the evidence for or against a model. To this end we plot the function $\alpha_N(\Pi) = F_B^*(\sqrt{N}(\hat{M}^2 - \Pi))$ for $\Pi > 0$, i.e. the value of $\alpha_N(\Pi)$ is given by the probability that the random quantity $X = \sqrt{N}(\hat{M}_*^2 - \hat{M}^2)$ is smaller than $\sqrt{N}(\hat{M}^2 - \Pi)$. Note that this implies that for Π increasing $\alpha_N(\Pi)$ decreases, because we then evaluate the cumulative distribution function $F_B^*(x)$ for decreasing x , and in particular, if $\alpha_N(\Pi)$ is small, at the left tail of F_B^* . We present the P -value curves for the parametric models A-D in Fig. 4.

The interpretation of the function $\alpha_N(\Pi)$ is as follows. Assume the true distance between a parametric model and the "true" density $K\rho$ is $M^2 = \Pi$. Now we reject the hypotheses $H : M^2 > \Pi$ (vs. alternative $M^2 \leq \Pi$) whenever $\alpha_N(\Pi) \leq \alpha$ for a given level of significance α . Hence $1 - \alpha_N(\Pi)$ can be regarded as the estimated evidence in favour of the parametric model U (up to a distance between parametric model and true density $M^2 \leq \Pi$). Finally the astrophysicist has to decide whether a value of $M^2 = \Pi$ should be regarded as scientifically negligible or as deviation from the "true" density $K\rho$ which is considered as significant by astrophysical reasons. For a more thorough introduction into P -value curves in the astrophysical context see [BM2], and for the statistical theory see Munk (2002) Sect. 5 and the references given there.

With this interpretation in mind we now determine "distance margins" from the P -value curves in Fig. 4. These margins indicate the most likely distance between the true density and the individual parametric models. We use those distances Π where the error probability for the hypothesis "the distance between parametric model and true density $K\rho$ is larger than Π " is $\approx 95\%$ and $\approx 5\%$ to define

the upper and lower bound of the distance margins (confidence interval), and find $6.5 \leq M^2 \leq 20.6$ for model A, $7.7 \leq M^2 \leq 22.5$ for model B, $5.1 \leq M^2 \leq 20.9$ for model C, and $6.3 \leq M^2 \leq 16.7$ for model D.

Observe that our distance margins are much more meaningful than, say, computing the “classical” χ^2 -distance between parametric model and data. This is in particular because the distance margins not only give the absolute distance between the parametric model and the non-parametric one, but also error bounds for the distance. Furthermore, our method allows and adapts for the commonly poorly known and heteroscedastic distribution of observational noise - in contrast to classical χ^2 -methods.

It is important to comment on the validity of our approach of using the non-parametric model as an “objective standard of measurement” in the context of the quality of the non-parametric model. To this end we consider two extreme cases. First, assume that the non-parametric model would fit the data rather bad relative to the estimated local standard deviation $\hat{\sigma}(l, b)$. In consequence the cumulative distribution function of $\hat{M}_{(i)}^2$ tends sharply to 1. This implies a P -value curve which goes to zero very quickly, and we have to conclude that the distance between parametric model and “true” density $K\rho$ is very small, and hence there is no reason to prefer non-parametric over parametric modelling of the data. On the other hand, now assume that the non-parametric model is a (nearly) perfect fit to the data relative to the local standard deviation. Then the cumulative distribution function of $\hat{M}_{(i)}^2$, i.e. of the estimated distance between parametric model and “true” density, tends very slowly to 1, implying a P -value curve which decreases to zero rather slowly. In this case we cannot make any statement about a small distance of the parametric model from the “true” density. In conclusion our new method even remains valid for “bad” non-parametric models serving as “objective standards of measurement”.

We now use the distance margins to answer our first question - whether the non-parametric model should be preferred over the parametric models. To this end we have to decide whether we consider the determined distance margin between a parametric model and the true density (here represented by the non-parametric model which is used as an objective standard of measurement) as astrophysically significant. For this we compare the distance margins with crude estimates for the distance between the non-parametric model and the *COBE/DIRBE* data on grid \mathcal{G} , and for the error dispersion in the *COBE/DIRBE* L-band data, as given by Spergel et al. (1995). If these latter values are smaller than the typical distance margins we conclude that the latter distances are astrophysically significant and the non-parametric model should be preferred.

We begin with the computation of the distance between the non-parametric model and the *COBE/DIRBE* data on the grid \mathcal{G} , normalized by the estimated variance of the *COBE/DIRBE* L-band data, which is $\approx 0.076^m$ (Spergel

et al., 1995, cf. Bissantz & Gerhard, 2002). This normalisation enables us to compare the above determined distances between the non-parametric model and the parametric models, observing that the quantity \hat{M}^2 is similar in construction to a rms difference between the models (on the sky), “weighted” by the local variance of the data $\hat{\sigma}^2(l, b)$. We find 0.62 for our crude estimate of the distance between the reference non-parametric model and the observed data. This, and in particular the normalized dispersion of the data (which by our definition amounts to 1), is significantly less than the distance margins indicate for the parametric models. Thus we conclude that the non-parametric model improves significantly over the parametric models and should be preferred.

This conclusion is supported by Fig. 5 where the squared (rms) residuals between the reference non-parametric model and the *COBE/DIRBE* L-band map, and the same for the best parametric models $\rho_{\hat{\sigma}}$ (the best of which is of type D, cf. Fig. 3), are compared. Obviously the non-parametric model fits the data very well, in particular in the central region $|l| \leq 50$ deg, $|b| \leq 20$ deg. The residuals of the parametric model, however, show systematic deviations from the data. Note, however, that the P -value curves provide us with substantially more information than these maps of model residuals, because they guard us against overfitting in a quantitative way.

Having decided that the distance margins are of astrophysical significance we proceed to the second question, which is to compare the parametric models among each others. This will be done for illustrational purpose mainly, because we have already seen that a non-parametric model should be preferred. To this end we use the right tail of the P -value curves, where $\alpha_N(\Pi_r) \approx 0.05$, i.e. we determine the distance Π_r for which the hypothesis “the distance between the parametric model and the true density $K\rho$ is larger than Π_r ” has an error probability $\approx 95\%$. Inspection of Fig. 4 shows that the intermediate model D outperforms the other parametric models because Π_r is smallest for this model, indicating that it is the best among models A-D. The 2- and 4-armed models A and C are approximately similar in quality, and the model without spiral arms (B) is clearly the worst. We remark that the differences between the distances Π_r for the models (as given by the upper bound of the distance margins, cf. above) are significantly larger than the normalized distance between the non-parametric model and the data, and in particular than the normalized dispersion in the data. We conclude that the differences between the models are significant, and that the intermediate model D is best, i.e. we can exclude a large distance of the parametric model from the true MW density with a higher level of confidence for model D than for models A-C.

Finally, we comment on the P -value curve analysis in the context of “classical” statistical tests, which start off from the hypothesis $\Pi = 0$. Fig. 6 presents the left tail of our P -value curves, where $\Pi \approx 0$, showing that some of the P -value curves intersect. This has an interesting consequence: a

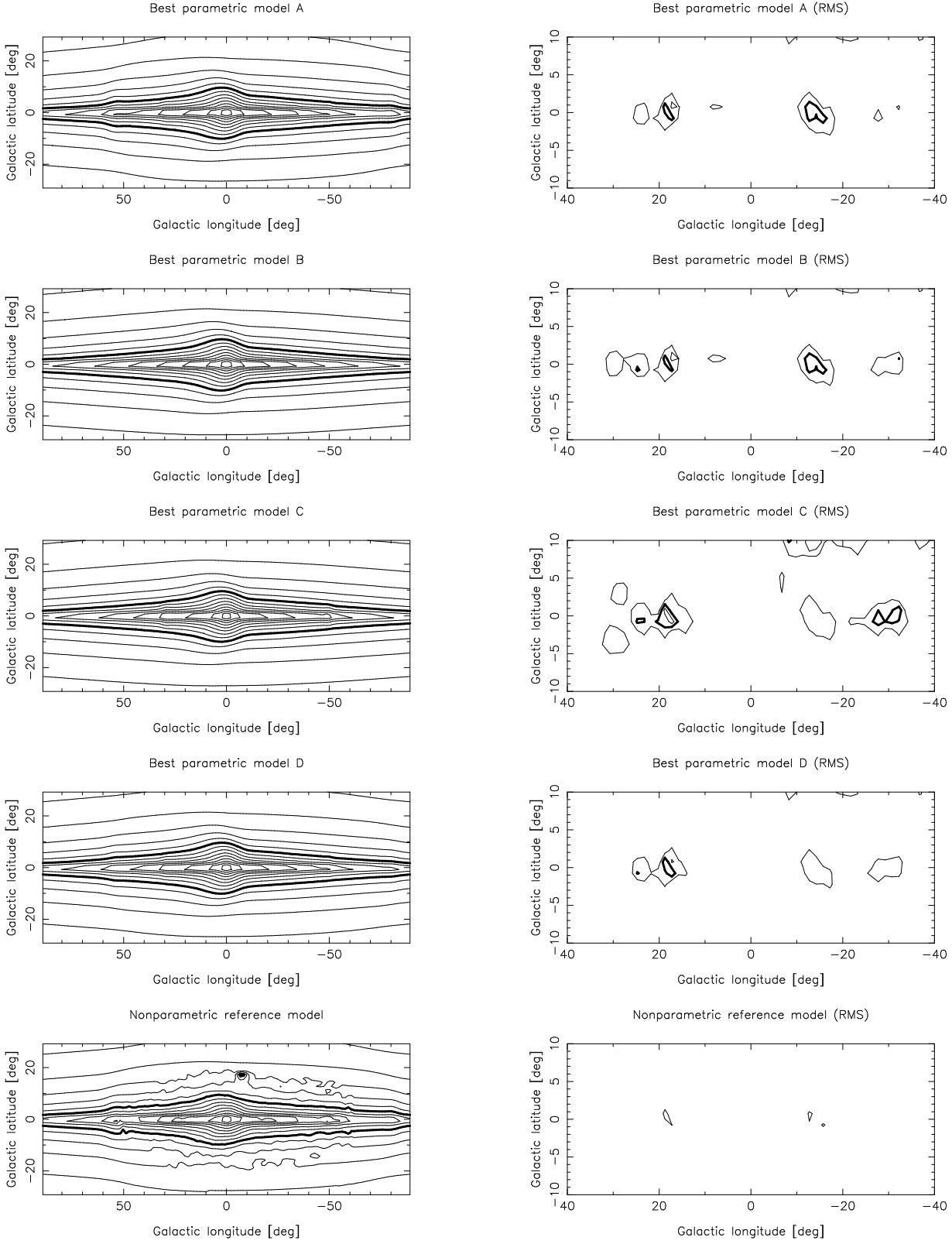


Figure 5. Square (rms) difference between the best-fitting parametric models ρ_{β} and the *COBE/DIRBE* L-band data, and the same difference for the reference non-parametric model. Contour spacing is 0.05mag^2 and the bold contour is at 0.1mag for for the rms plots (left hand side) and 0.5mag , 0mag^2 for the model plots (right hand side). Contour lines in the rms plots have been smoothed by averaging over a point and its four nearest neighbours. Different areas of the sky are shown for the rms plots (the region of sky to which the parametric models were fitted) and the model plots (full sky area covered by our *COBE/DIRBE* map). Note the different appearance of spiral arm tangent points for the different models, and the corresponding residuals in the rms maps.

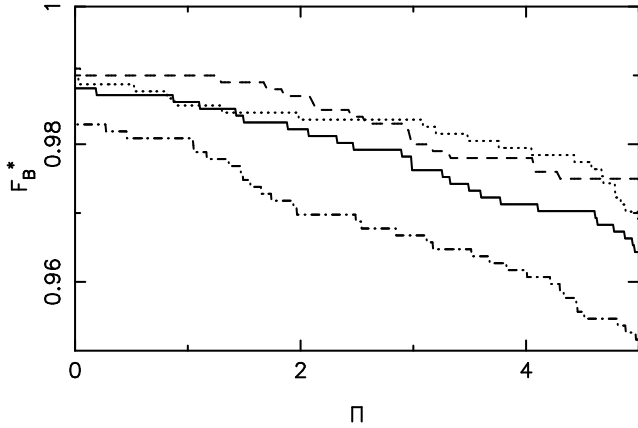


Figure 6. P -value curves $\alpha_N(\Pi) = F_B^*(\hat{M}^2 - \Pi)$ for models A (full line), B (dashed), C (dot-dash-dot-dash), and D (dotted), respectively, where $\Pi \approx 0$.

”classical” test based on the hypothesis that the model holds ($\Pi = 0$) leads to a different answer (here: model C performs best) than our proposed method, which is based on the more realistic hypothesis, that there is a nonzero distance $\Pi > 0$ between the parametric model and the true MW density $K\rho$. Observe that, because we have found in our precedent analysis that the observed distances between the parametric models and the true MW density are significant, a classical test would indeed be inappropriate in our application.

To close this section we summarize the answer to our questions raised at the beginning of this section:

- (i) The non-parametric model should be preferred over the parametric models because the improvement in fit is astrophysically relevant and with high confidence due to systematic features.
- (ii) A parametric model with 4-armed spiral structure, however, with reduced amplitude of the Sagittarius-Carina arm and its counter-arm as suggested by Drimmel & Spergel (2001), significantly outperforms the other parametric models. The worst performance is shown by a model without spiral arms at all as to be expected.

6 DISCUSSION

We have suggested a resampling algorithm to assess the necessity of non-parametric instead of parametric modelling in astrophysical (inverse) regression problems. By means of this we are in the position to decide whether the deviations between the parametric model and the data are systematic or due to noise. Furthermore our method can be used to select the best among several competing parametric models. Our approach is based on the idea to investigate the statistical behaviour of the estimated distance between the true model ρ and the artificial model U under all ”possible worlds” $M^2 = \Pi$, and not only when $M^2 = 0$ (i.e. ρ and U coincide), as classical goodness of fit tests do. Moreover, we

compare all parametric models by relating them to a non-parametric ”super-model” which can be validated itself by our method.

To illustrate our method we have applied it to the problem of recovering the near-infrared luminosity density distribution of the Milky Way from a dust-corrected *COBE/DIRBE* L-band map (Spergel et al., 1995). In this paper we have focused on the morphology of the spiral arms, comparing parametric models which have zero, 2 or 4 spiral arms, and also an ”intermediate” 4-armed model, in which the Sagittarius-Carina arm and its counter-arm are considerably less strong than the other pair of arms. These parametric models have been compared with a non-parametric model of Bissantz & Gerhard (2002). From our statistical analysis we conclude that the non-parametric model is significantly better than the parametric models and hence should be preferred. This is due to systematic departures between data and parametric models, which are in particular to inflexible to reproduce certain deviations from a double-exponential disk and smooth spiral arms. Furthermore, we have found that the ”intermediate” parametric model outperforms the other parametric models by a significant amount. Thus, from the analysis of the dust-corrected *COBE/DIRBE* L-band map, a parametric model of the Milky Way with 4-arms, but the Sagittarius-Carina arm (and in our model also its counter-arm) of reduced amplitude - similar to the suggestion of Drimmel & Spergel (2001) - is to be preferred over models with 2-armed or 4-armed structure, and in particular over a model without spiral structure, which performed worst in our analysis.

Before making our final conclusions we want to point out some difficulties of the *COBE/DIRBE* NIR data with respect to spiral arm analysis as pointed out by a referee. Firstly, dust extinction, which is biased towards the spiral arms, makes those less evident in NIR data (cf. Drimmel & Spergel, 2001). Our analysed L-band map was dust-corrected by Spergel et al. (1995), but this extinction-bias obviously also results in their dust-correction being more difficult to perform. Secondly, the large angular size of the nearby Sagittarius-Carina arm makes it more difficult to observe in NIR maps, because combined with the small instrument beam a larger amount of emission will be lost below the sensitivity threshold of the instrument than for the other arms. Finally, since we had to restrict our parametric fitting to a range of longitudes $|l| \leq 40$ deg of the data due to computational reasons (range of the non-parametric model), we did not include the tangent point regions of the Sagittarius-Carina arm, which substantially weakens any conclusion regarding a differing amplitude of this arm. The latter two points obviously weaken the statistical evidence for the intermediate model compared to the 4-armed model by some amount.

This result is consistent with Drimmel & Spergel (2001), and also with the SPH models of the inner Milky Way gas dynamics of Bissantz & Gerhard (2002), who found that 4-armed spiral structure is needed in the gravitational po-

tential caused by the stellar distribution. They analysed the gas flow in a potential ("mix"), which is quite similar to our intermediate model. This gas model was found to be slightly worse than gas flow models in their standard 4-armed potential, but not nearly as bad as the gas flow in 2-armed potentials, and is clearly still acceptable.

7 ACKNOWLEDGMENTS

We are grateful to O.Gerhard and H.Dette for helpful comments, and thank the anonymous referees for thoughtful suggestions which lead to a clearer presentation of our result. The source code of our method can be obtained from the authors on request. Please send an e-mail to bissantz@math.uni-goettingen.de

REFERENCES

- Binney J., Gerhard O., Spergel D., 1997, MNRAS, 288, 365 (BGS)
- Bissantz N., Englmaier P., Binney J., Gerhard O., 1997, MNRAS, 289, 651
- Bissantz N., Gerhard O., 2002, MNRAS, 330, 591
- Bissantz N., Gerhard O., Englmaier P., 2002, in revision
- Bissantz N., Munk A., 2001, A&A, 376, 735 (BM1)
- Bissantz N., Munk A., 2002, MNRAS, 336, 131 (BM2)
- Burnham K.P., Anderson D.A., 1998, Model selection and inference. A practical information theoretic approach. Springer-Verlag, New York
- Dette H., 1999, Ann. Stat., 27, 1012
- Dette H., von Lieres und Wilkau C., Sperlich S., 2001, submitted
- Dette H., Munk A., 2002, Statistica Neerlandica, to appear
- Dette H., Neumeier N., 2001, Ann. Stat., 29, 1361
- Drimmel R., 2000, A&A, 358, 13
- Drimmel R., Spergel D.N., 2001, ApJ, 556, 181
- Dwek E., et al., 1995, ApJ, 445, 716
- Englmaier P., Gerhard O., 1999, MNRAS, 304, 512
- Eubank R., 1999, Nonparametric Regression and Spline Smoothing. Marcel Dekker, New York, Basel
- Feigelson E. D., Babu G. J., 2002, Proceedings of the conference on "Statistical Challenges in Modern Astronomy III". Springer-Verlag, New York
- Freudenreich H.T., 1998, ApJ, 492, 495
- Hocking R.R., 1996, Methods and Applications of Linear Models. Wiley, New York
- Lucy L.B., 1994, RvMA, 7, 31
- Magorrian J., et al., 1998, AJ, 115, 2285
- Munk A., 2002, Scand. Journ. Statist., 29, 501
- Munk A., Wagner T., Freitag G., 2001, Journ. Roy. Statist. Soc. Ser. B, in revision
- Ortiz R., Lépine R.D., 1993, A&A, 279, 90
- Pijpers F.P., Thompson M.J., 1994, A&A, 281, 231
- Pijpers F.P., Wanders I., 1994, MNRAS, 271, 183
- Press W.H., Teukolsky S.A., Vetterling W.T., et al., 1994, Numerical recipes in C (2nd ed.). Cambridge University Press, Cambridge
- Rix H.-W., Zaritsky D., 1995, ApJ, 447, 82
- Ruppert D., Wand M.P., Holst U., Hössjer O., 1997, Technometrics, 39, 262
- Spergel D.N., Malhotra S., Blitz L., 1995, in Minniti D., Rix H.-W., eds, Spiral Galaxies in the Near-IR. Springer-Verlag, Berlin, p. 128
- Stanek K.Z., Mateo M., Udalski A., et al., 1994, ApJ, 429, 73
- Stanek K.Z., Udalski A., Szymanski M., et al., 1997, ApJ, 477, 163
- Thompson A.M., Kay J.W., Titterton D.M., 1991, Biometrika, 78, 475
- Vallée J.P., 2002, ApJ, 566, 261
- Wand M.P., Jones M.C., 1995, Kernel smoothing. Monographs on Statistics and Applied Probability 60. Chapman & Hall, London
- Wahba G., 1990, Spline models for observational data. CBMS-NSF Regional Conference Series in Applied Mathematics, 59. Society for Industrial and Applied Mathematics, Philadelphia
- Wallington S., Narayan R., Kochanek C.S., 1994, ApJ, 426, 60
- Wallington S., Kochanek C.S., Narayan R., 1996, ApJ, 465, 64